Infrared spectroscopy of copper–resveratrol complexes: A joint experimental and theoretical study

ARTICLE *in* THE JOURNAL OF CHEMICAL PHYSICS · JULY 2012

Impact Factor: 2.95 · DOI: 10.1063/1.4732583 · Source: PubMed

6 AUTHORS, INCLUDING:

Maria Elisa Crestoni
Sapienza University of Rome
135 PUBLICATIONS **1,733** CITATIONS
SEE PROFILE

Simone Taioli
European Centre for Theoretical Studies in N…
43 PUBLICATIONS **579** CITATIONS
SEE PROFILE

Paolo Tosi
Università degli Studi di Trento
116 PUBLICATIONS **1,335** CITATIONS
SEE PROFILE

Infrared spectroscopy of copper-resveratrol complexes: A joint experimental and theoretical study

B. Chiavarino, M. E. Crestoni, S. Fornarini, S. Taioli, I. Mancini, and P. Tosi

Citation: The Journal of Chemical Physics **137**, 024307 (2012); doi: 10.1063/1.4732583
View online: http://dx.doi.org/10.1063/1.4732583
View Table of Contents: http://scitation.aip.org/content/aip/journal/jcp/137/2?ver=pdfcov
Published by the AIP Publishing

Infrared spectroscopy of copper-resveratrol complexes: A joint experimental and theoretical study

B. Chiavarino,[1] M. E. Crestoni,[1] S. Fornarini,[1] S. Taioli,[2,3,4,5] I. Mancini,[3] and P. Tosi[3]
[1]*Dipartimento di Chimica e Tecnologie del Farmaco, Sapienza - Università di Roma, Piazzale A. Moro 5, 00185 Rome, Italy*
[2]*Interdisciplinary Laboratory for Computational Science, FBK-CMM and University of Trento, Via Sommarive 18, 38123 Trento, Italy*
[3]*Department of Physics, University of Trento, Via Sommarive 14, 38123 Trento, Italy*
[4]*Istituto Nazionale di Fisica Nucleare, Sezione di Perugia, Italy*
[5]*Department of Chemistry, University of Bologna, Via F. Selmi 2, I-40126 Bologna, Italy*

(Received 13 March 2012; accepted 18 June 2012; published online 11 July 2012)

Infrared multiple-photon dissociation spectroscopy has been used to record vibrational spectra of charged copper-resveratrol complexes in the 3500–3700 cm^{-1} and 1100–1900 cm^{-1} regions. Minimum energy structures have been determined by density functional theory calculations using plane waves and pseudopotentials. In particular, the copper(I)-resveratrol complex presents a tetra-coordinated metal bound with two carbon atoms of the alkenyl moiety and two closest carbons of the adjoining resorcinol ring. For these geometries vibrational spectra have been calculated by using linear response theory. The good agreement between experimental and calculated IR spectra for the selected species confirms the overall reliability of the proposed geometries. © *2012 American Institute of Physics*. [http://dx.doi.org/10.1063/1.4732583]

I. INTRODUCTION

Resveratrol ((E)-5-[2-(4-hydroxyphenyl) ethenyl] benzene-1,3-diol) is a hydroxylated stilbene present in grapes, nuts, peanuts, and some plants used in traditional pharmacopoeia such as *Polygonum cuspidatum*, from which it is extracted to prepare nutritional supplements. Being a minor component of red wines (0.1–8 mg/l) it is considered responsible for the beneficial health effects attributed to moderate wine consumption. In fact many valuable properties are attributed to resveratrol,[1] in particular antioxidant, anticarcinogenic, and antinflammatory activities. Most interestingly, resveratrol has been demonstrated to regulate various proteins and in particular it directly inactivates phosphodiesterase enzymes (PDEs), leading to a signaling cascade that activates Sirtuin1 (SIRT1).[2] Because the expression of SIRT1 is linked to calorie restriction effects on life-span extension, resveratrol has been suggested as a mimetic of calorie restriction, a well known way to prevent aging.[3] This implication has increasingly attracted the interest of both the scientific community as well as the parapharmaceutic industry.[4]

However, it should not be forgotten that molecules normally acting as antioxidants can also exert prooxidant properties by reducing metal ions, which can then produce reactive oxygen species. The prooxidant mechanism of resveratrol is based on the acidity of the phenol group, involving a proton loss from the OH in para position, to give a phenoxide anion which reacts with Cu(II) ion producing Cu(I). This latter ion is then involved in redox reactions with oxygen species, whose final products are Cu(II) and oxygen radicals.[5] It is therefore important to investigate the interaction between metal ions and resveratrol. A recent paper reported for the first time the detection of resveratrol-copper complexes by electrospray ionization (ESI).[6] The structure of these complexes can be investigated by vibrational spectroscopy. In the present work we used infrared multiple-photon dissociation (IRMPD) spectroscopy to perform such a task. IRMPD spectroscopy is an action spectroscopy in which the response of the molecule to photon absorption is recorded rather than the direct absorption of the incident light.[7] It is based on the use of IR laser radiation of high fluence and broad tunability. When the energy of the photon flux is resonant with an active vibrational mode of the sample, a multiple sequence of events comprising photon absorption by the investigated mode and fast energy redistribution increases the vibrational energy reaching a fragmentation threshold. The dependence of the fragmentation yield on the photon wavenumber generates an IRMPD spectrum revealing the IR absorption features of the assayed species. Action spectroscopy is a viable spectroscopic probe for gaseous ions whose typically low density number does not allow performing direct absorption spectroscopy. In this way, IRMPD spectroscopy has provided valuable contributions in the past decade in elucidating the structural and electronic features of organometallic complexes or metal ion cationized organic molecules.[8–11]

IRMPD spectroscopy is used in this work to investigate the 1:1 and 1:2 copper (I) complexes with resveratrol, henceforth denoted $[Cu(Resv)]^+$ and $[Cu(Resv)_2]^+$, respectively. In addition, the investigation has included ionized resveratrol ($(Resv)^{+\bullet}$) and the copper(I) complex with dihydroresveratrol (5-(4-hydroxyphenethyl)benzene-1, 3-diol, henceforth referred to as DHResv). In the latter complex, $[Cu(DHResv)]^+$, also comprised in the previous report,[6] the flexible $–CH_2–CH_2$ chain connecting the two aryl rings allows a folded structure whereby the metal ion can interact with the two aromatic rings, embedded between them. The scope of the present investigation, besides providing IR

signatures for the selected species in an isolated state, aims at linking the experimental IRMPD spectra with the plausible structures of the sampled ions.

To this end calculations of the IR spectra have been performed within the framework of density functional theory (DFT). This approach, along with the plane wave (PW) expansion of the molecular orbitals, allows us treating the different complexes investigated in this work at the same level of accuracy, and to include the dispersion forces. On this respect, molecular vibrational properties can be calculated using two different approaches: by diagonalizing the dynamical matrix or by applying linear response theory. In the former approach, the energy gradient with respect to atomic displacements is usually computed analytically by using the Hellmann–Feynman theorem, while second derivatives are computed as numerical derivatives of energy gradients using the central difference formula. Therefore, within this method one has to test the size of the displacement to be used in the calculation of the force constant matrix, which is given by

$$D_{\alpha,\beta}(i,j) = -\frac{1}{\sqrt{(m_i \times m_j)}}\phi_{\alpha\beta}(i,j), \qquad (1)$$

where i, j identify the atoms i and j, $\phi_{\alpha\beta}(i,j)$ is the force constant matrix, and m_i, m_j are the masses of atoms i and j. The displacement has to be small in order to be in the validity range of the harmonic approximation, but also big enough so that the forces induced in the molecular complex are not too small compared to the numerical noise in the calculations. Finally, one calculates eigenvalues and eigenvectors of the dynamical matrix to be directly compared with experimental spectra available from infrared absorption spectroscopy. Intensities are finally found by applying dipole approximation. To obtain good quality spectra, extremely accurate total energies must be found and extensive checks on the size of the atomic displacement have to be performed. Therefore, in order to calculate the second derivatives to obtain vibrational frequencies and intensities of resveratrol-based molecular complexes we preferred to use density functional perturbation theory (DFPT),[12] also referred to as linear response (LR) theory. In this case, tests on the resveratrol molecule showed that frequencies and intensities do not depend critically on the value of the displacement. This paper is structured in the following way. In Sec. II we outline the experimental apparatus and methods used to record the IRMPD spectra. In Sec. III we briefly describe the *ab initio* theoretical and computational approaches to the problem that we propose here. The experimental results and comparison with the ensuing calculations of the infrared spectra of a number of proposed resveratrol-copper complexes within DFPT approximation are finally illustrated in Sec. IV.

II. EXPERIMENTAL METHODS

The ions of interest are generated by electrospray ionization (ESI) of an approximately 1:1 resveratrol(DHResveratrol)/$CuSO_4$ solution (10^{-4} M) in a 50/50 mixture of methanol and water using direct infusion by a syringe pump. Resveratrol and $CuSO_4$ were supplied by Sigma Aldrich Co. (St. Louis, USA). Dihydroresveratrol was prepared by hydrogenation of resveratrol.[6] Typical ESI parameters are an infusion flow rate of 180 μl/h, a spray voltage of 4500 V and a capillary temperature of 300 °C.

IRMPD experiments on the sampled species are performed using two experimental platforms with different laser systems. The 1100–1900 cm^{-1} region has been explored using the free electron laser (FEL) beamline at the CLIO (Centre Laser InfraRouge, Orsay) center. The FEL system is based on a 16–48 MeV linear electron accelerator where bunches of electrons are injected in the alternating magnetic field placed in the optical cavity. Wavelength tunability of this laser system is achieved at fixed electron energy by changing the gap between magnets. For the experiments in the 1100–1900 cm^{-1} spectral region, the electron energy was fixed at 45 MeV and a stable average power of 1 W was observed. The IR FEL delivers 8 μs long trains of macropulses at a repetition rate of 25 Hz. Each macropulse conveys typical energies of 40 mJ. The laser-wavelength profile was monitored while recording the spectra with a monochromator associated to a pyroelectric detector array. The bandwidth of IR-FEL is 0.4%–0.5% of the central wavelength.

The FEL-based experiment was performed using a modified Bruker Esquire 3000 Paul-trap type mass spectrometer with a conical hole in the ring electrode allowing the optical access to the center of the trap.[13] The commercial Bruker Esquire software was used in the experiment. The ions of interest were mass-selected in the MS1 step and the control of the irradiation time (typically 1 s) was obtained using the MS2 step. In the case of $[Cu(Resv)]^+$, the species was obtained in the MS2 step by dissociation of $[Cu(Resv)_2]^+$, and was then submitted to irradiation in the MS3 step for 2 s. Mass spectra were averaged over 10 accumulations and the sequence repeated for 6 times at each recorded frequency.

An optical parametric oscillator/amplifier (OPO/OPA) (LaserVision) coupled to a Paul ion trap tandem mass spectrometer Esquire 6000+ (Bruker Inc.) is employed to explore the 3500–3700 cm^{-1} spectral region of the different species under study.[14] This parametric converter is pumped by a non seeded Nd:YAG laser (Continuum Surelite II) operating at 10 Hz repetition rate. The typical pulse width of this pump laser is 4–6 ns with output pulse energy of 600 mJ at 1064 nm. Tunability is achieved by angle tuning of OPO and OPA crystals simultaneously using software controlled stepping motors. The typical output energy from the OPO/OPA laser was 22 mJ/pulse in the spectral range of investigation with 3–4 cm^{-1} bandwidth. The mid-IR output from OPO/OPA is steered in the ion trap using a gold coated plane mirror and is focused loosely using an MgF_2 lens of focal length 37 cm. The IR beam focusing is performed to achieve better overlap with the trapped ion cloud. In the trap, ions were accumulated for 10 ms prior to IR irradiation which was allowed to last 0.5–2 s. Once again, multistage mass spectrometry is performed using the standard Bruker Esquire Control (v5.2) software.

IRMPD spectra are obtained by plotting the photofragmentation yield R ($R = -\ln(I_{parent}/[I_{parent} + \sum I_{fragment}])$), where I_{parent} is the intensity of the parent ion and $\sum I_{fragment}$

is the sum of the intensities of fragment ions as a function of the IR radiation wavenumber.

III. THEORETICAL AND COMPUTATIONAL METHODS

Calculations have been performed within the framework of DFPT using the *ab initio* total energy and molecular dynamics program VASP.[15–17] The ion-electron interaction has been described using the projector augmented wave (PAW) technique,[18–20] in which the explicit treatment of core electrons is replaced by atom-centered augmentation spheres within a given ionic radius and by envelope functions outside such spheres. Single-particle orbitals are expanded in plane waves (PWs). In principle, electron orbitals may be expanded in term of any convenient basis set, be it Gaussians (GTO) or PW. While Gaussian functions have been used in a large number of code suites, such as Gaussian[21] or GAMESS,[22] for the simulation of molecular properties, notably the vibrational frequencies, in this work we decided to use the latter for two reasons.

First, we study a variety of resveratrol-copper complexes at different levels of aggregation. On this respect, while Gaussian basis sets need to be tailored for any specific application and may suffer basis set superposition errors (BSSEs), the use of PW ensures the same level of accuracy irrespectively of the dimensionality of the system as accuracy depends only on the energy cutoff.

Second, we use LR theory to calculate both the normal mode eigenvectors and the Born effective charge tensors for the assessment of the vibrational intensities. The use of PW on this respect presents the advantage of simplifying the calculation of the Hellmann–Feynman forces as Pulay forces are zero by construction.

Finally, a principal difference between all-electron GTO implementations of DFT and PW approaches is the use of pseudopotential, which acts as an effective interaction between valence electrons and ions, while core-electrons are frozen in the core. Tosoni *et al.*[23] showed that the use of PW in connection with PBE (Ref. 20) and PW91 (Ref. 24) pseudopotentials compares very well with GTO-based approaches for calculating structures, binding energies, and harmonic vibrational spectra of the formic acid molecule in the free-gas phase. Furthermore, PW performs much better in the molecular crystal phase to assess binding energies likely due to larger BSSE in this phase. In particular, the results of the frequency calculation involving the O–H stretching mode at around 3600 cm^{-1}, which is of interest in our work, are improved in accuracy by increasing from one side the energy cut-off of the PBE pseudopotential from 110 to 130 Ry and from the other side by enlarging the GTO basis set from 6-311G(d,p) to TZP. Harmonic frequencies are quite poor with small size GTO basis set, with discrepancies higher than 100 cm^{-1} in comparison to Triple-Zeta Polarization (TZP) basis set. Counterpoise corrections proved to be crucial to obtain well converged results for molecular crystals containing hydrogen and first-row elements. For frequencies involving intramolecular normal modes the agreement is better.

Karhánek *et al.*[25] performed the vibrational analysis of methanetiol (CH_3SH) and methyl thiolate (CH_3S^-) in the gas phase by using both PW91 and B3LYP (Ref. 26) exchange-correlation functional in connection with 6-311G(d) GTO basis set as implemented in GAUSSIAN. These results were compared with PW-DFPT calculations using PW91 pseudopotential for 400 eV energy cut-off. In this case, even larger discrepancies are found between the two approaches. For both molecules, the PW approach shows much better agreement than GTO-based methods with available data for the stretching, deformating, and rocking modes and the C–S stretching mode. In particular, for the two almost degenerate asymmetric O–H stretching modes, which are of importance even in our work, the frequencies calculated by using GAUSSIAN are as higher as 100 cm^{-1} on respect to the values obtained by using LR theory, a difference too high to be attributed to anharmonic effects only. Furthermore, large discrepancies have been found in the relative intensity of the modes between PW- and GTO-based approaches. For a comparison between the spectra of the complexes investigated in this work obtained at this level of theory with those obtained by using more standard GTO-based DFT calculations see supplementary material.[27] In the latter, B3LYP exchange-correlation potential for the copper-resveratrol complexes along with a 6-31G* GTO basis set (6-311G** for $Res^{+\bullet}$) have been used. The main source of discrepancies between GTO and PW approaches for calculating IR spectra on resveratrol-Cu complexes is mainly the need of rescaling the frequencies in the former case.

In order to test PW-based approach for our system, we decided to apply LR theory for simulating the structures and relative stabilities of a phenol-copper cation for different copper binding sites, on the aromatic ring and on the oxygen atom, respectively. In this case-study we tested different exchange-correlation functionals and various PAW pseudopotentials. These calculations aim at the assessment of the DFT parameters to be used in the study of the binding of copper on more complex systems, notably copper-resveratrol complexes.

The kinetic energy cutoff is set to 500 eV, which ensures convergence of the structural parameters of phenol complexes to better than 0.05% with respect to available experimental data.[28] Spin-orbit and fully non-collinear magnetic effects have also been tested without finding appreciable difference in the structural parameters, notably binding site and bond length, with respect to the case in which they are not included. Calculations have been performed at Γ point. The simulation cell is cubic with a linear dimension of 12 Å.

The resulting configurations obtained for different binding sites of the copper atom are plotted in Fig. 1 in order of increasing energy from (a) to (e). The figure clearly shows that the copper ion preferentially sits on the top of the ring, while unfavorably it binds with the oxygen lone pairs, as one could rather expect from chemical analysis. The differences in energy among the most stable configuration (see Fig. 1(a)) and the other structures are 0.018, 0.025, 0.054, and 0.083 eV, respectively. The first three structures are therefore almost degenerate within chemical accuracy, with the copper-to-carbon bond length equal to 2.11 Å in the most stable configuration. These preliminary results have been obtained by using PBE-GGA (Ref. 20) pseudopotential. Within local density approximation (LDA) (Ref. 29) we obtain a slight

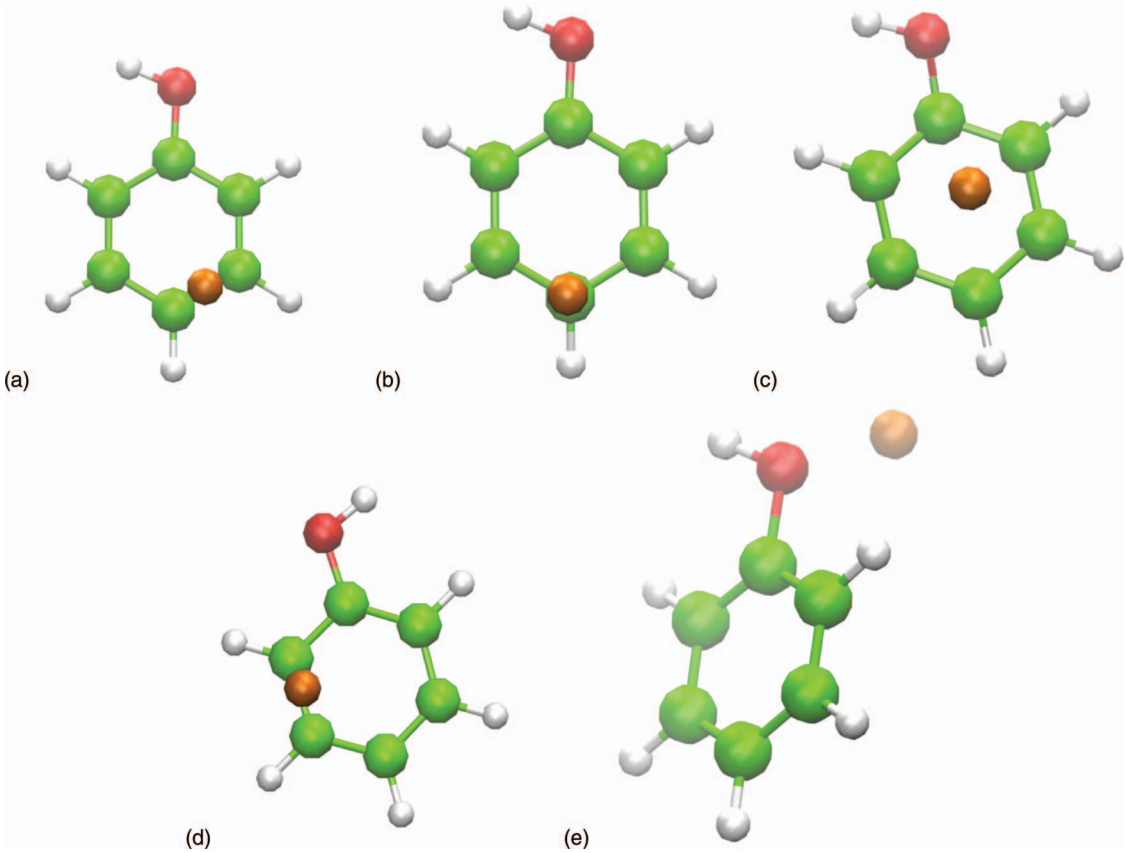

FIG. 1. Optimized structures of phenol complexes for different binding sites of the copper(I) atom. Carbon is in green, hydrogen in gray, copper in orange, oxygen in red.

decrease of about 0.3% of the carbon to copper bond distance, as expected since PBE usually overestimates the bond length, particularly for hydrogen bonds.[30] We also tested these PAW potentials with the 3*p* either frozen in the core, or explicitly included in valence, along with the 3*d* and 4*s* electrons. After these tests, we decided to use the PBE-GGA (Ref. 20) functional in all further calculations, the PAW potential without 3*p* electrons in valence, and to neglect spin-orbit interactions. Our prediction on the copper ion binding site above the aromatic ring is in good agreement with simulations performed by Milko *et al.*[28] on the same system using coupled cluster (CCSD(T)) extrapolated to the basis set limit. A second goal of this work is the vibrational analysis of resveratrol-copper molecular complexes to be compared with our IRMPD spectra. To perform these calculations, we used linear response DFPT (LR-DFPT), whose detailed description is reported in the Appendix for the sake of completeness.

IV. RESULTS

A. IRMPD spectroscopy

Fig. 2(a) shows the IRMPD spectrum of the radical cation $(Resv)^{+\bullet}$, obtained by plotting the photofragmentation yield versus the IR radiation wavenumber in the 1100–1900 cm^{-1} spectral region. The radical cation of resveratrol has been obtained by electrospray ionization from a 1:1 resveratrol/$CuSO_4$ solution 10^{-4} M in methanol/water (1:1) and an exemplary mass spectrum is shown in Fig. S1 of the supplementary material.[27] $(Resv)^{+\bullet}$ ions at *m*/*z*228 (where *m*/*z* for an ion is the ratio between its mass in atomic mass unit (a.m.u.) and its charge expressed as the number of elementary charges) yield fragment ions at *m*/*z*211, *m*/*z*199, and *m*/*z*182 when irradiated with the FEL beam tuned in resonance with an active vibrational mode of the parent ion. The same fragmentation products are observed in the electron ionization mass spectrum of *trans*-resveratrol.[31] The major features in the IRMPD spectrum in the mid IR region are observed at 1156, 1323–1343, and 1573 cm^{-1}. The IRMPD spectrum in the 3500–3700 cm^{-1} region shows two distinct bands at 3601 and 3643 cm^{-1} (see Fig. 3(a)).

In the IR spectrum of the neutral molecule in KBr pellet the νOH bands yield a broad and intense absorption with the νOH of the hydroxyl group in para position assigned at 3380 cm^{-1} and the in-phase and anti-phase coupled νOH of the dihydroxyphenyl group assigned at 3397 and 3405 cm^{-1}, respectively.[32] However, given the possible pronounced intermolecular interactions in the solid sample, any relationship between the IR spectrum of the neutral and the one of the radical cation is subject to several factors, not easy to predict.

Fig. 2(b) shows significant features of the IRMPD spectrum of the copper(I) complex of resveratrol, $[Cu(Resv)]^+$, recorded in the 1100–1300 and 1500–1600 cm^{-1} wavenumber ranges. The photofragmentation process proceeds mainly by formal loss of Cu and water as neutral fragments giving $C_{14}H_{10}O_2^+$ product ion. The $[Cu(Resv)]^+$ complex is obtained by collision induced dissociation of the Cu(I) complex with two *trans*-resveratrol ligands and is remarkably stable

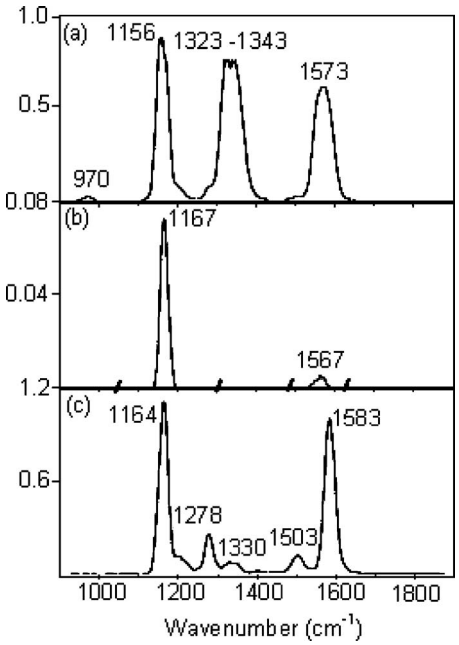

FIG. 2. IRMPD spectrum of $(Resv)^{+\bullet}$ (a), $[Cu(Resv)]^+$ (b), and $[Cu(Resv)_2]^+$ (c) in the 1000–1800 cm^{-1} wavenumber range. To be noted, the IRMPD spectrum of $[Cu(Resv)]^+$ has been recorded in the 1100–1300 and 1500–1600 cm^{-1} wavenumber ranges.

against photodissociation, when compared with $(Resv)^{+\bullet}$ ions for example, and required an exceptionally long irradiation time (2 s) in order to observe any IRMPD activity. However, the bands at 1167 and 1567 cm^{-1}, searched in a region where pronounced activity was expected, are clearly characteristic features for this species. In the νOH region a sharp band at 3628 cm^{-1} can be observed, midway between the two absorptions displayed by $(Resv)^{+\bullet}$ ions (Fig. 3(b)). The copper(I) complex with two resveratrol ligands yields $[Cu(Resv)]^+$ and $[Cu(Resv)(H_2O)]^+$ as photofragmentation products and displays the IRMPD spectrum reported in Fig. 2(c). The most active modes at 1164 and 1583 cm^{-1} share similar resonances with likely corresponding modes of the $[Cu(Resv)]^+$ complex. In between these two pronounced bands the IRMPD spectrum in the fingerprint region shows a complex structure with several features of significant intensity. The OH stretching region is characterized by a sharp band at 3643 cm^{-1} (see Fig. 3(c)).

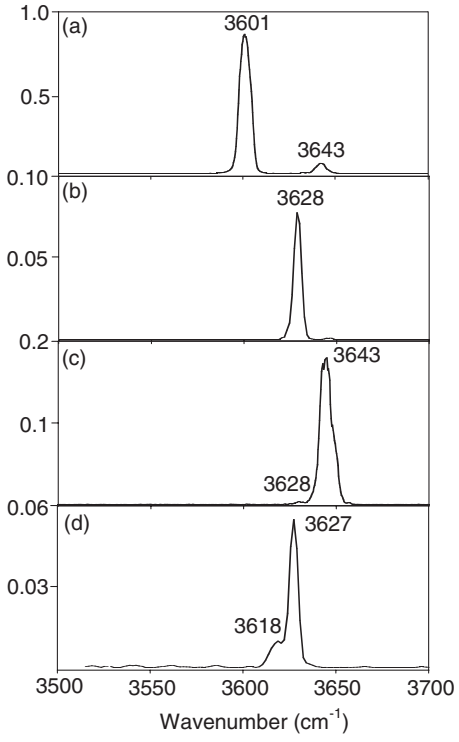

FIG. 3. IRMPD spectrum of $(Resv)^{+\bullet}$ (a), $[Cu(Resv)]^+$ (b), $[Cu(Resv)_2]^+$ (c), and $[Cu(DHResv)]^+$ (d) in the 3500–3700 cm^{-1} wavenumber range.

In both Figs. 3(b) and 3(c) we see only one significant band. However, very weak motifs (~2% in the relative intensity) on the blue and red side of the bands at 3628 and 3643 cm^{-1}, respectively, can be observed. They are likely not artifacts but can be associated to the presence of minor isomers. They will not be given further notice because of their negligible abundance.

The IRMPD spectroscopic investigation of the 1:1 complex of Cu(I) with dihydroresveratrol, examined in the 3500–3700 cm^{-1} range, presents a composite feature with a sharp maximum at 3627 cm^{-1} and an unresolved shoulder at 3618 cm^{-1}. Three weak features appearing from 3530 to 3590 cm^{-1} are mere artifacts and should be attributed no real meaning.

B. Theoretical results and comparison with experiments

The parameters used in the calculation of the ground-state structures and of the optical properties of resveratrol and resveratrol-copper complexes have been fixed to those found from the previous test on the phenol-copper complex. After convergence tests, the atomic displacement has been finally chosen equal to 0.05 Å. The kinetic energy cut-off is 500 eV, ensuring convergence of the structural parameters of resveratrol and resveratrol complexes to better than 0.05% with respect to available experimental data.[6] The structures have been relaxed to obtain forces below 10^{-3} eV/Å, an accuracy needed for the rigorous assessment of the vibrational frequencies and intensities. The linear dimension of the simulation cubic cell was increased from 12 Å for the pristine resveratrol molecule to 20 Å for the largest complexes to avoid spurious interactions among periodic images.

The resveratrol-copper topological analysis starts from our previous finding that the copper adsorption position on phenol is not close to the oxygen as one could argue by relying only on chemical intuition. Rather copper sits on the top of the carbon atoms. The same conclusion has been drawn for resveratrol and, thus, we placed the copper atom on several adsorption sites coordinating with carbon atoms, for example in the middle-top of the phenol ring, on the top of a single carbon atom and bound with two carbon atoms of the alkenyl moiety and two closest carbons of the adjoining resorcinol ring. DFT structural optimization procedures were based initially on a temperature-constrained *ab initio* molecular dynamics in order to find a reasonable starting guess for a quasi-Newton (variable metric) algorithm used to relax the ions into

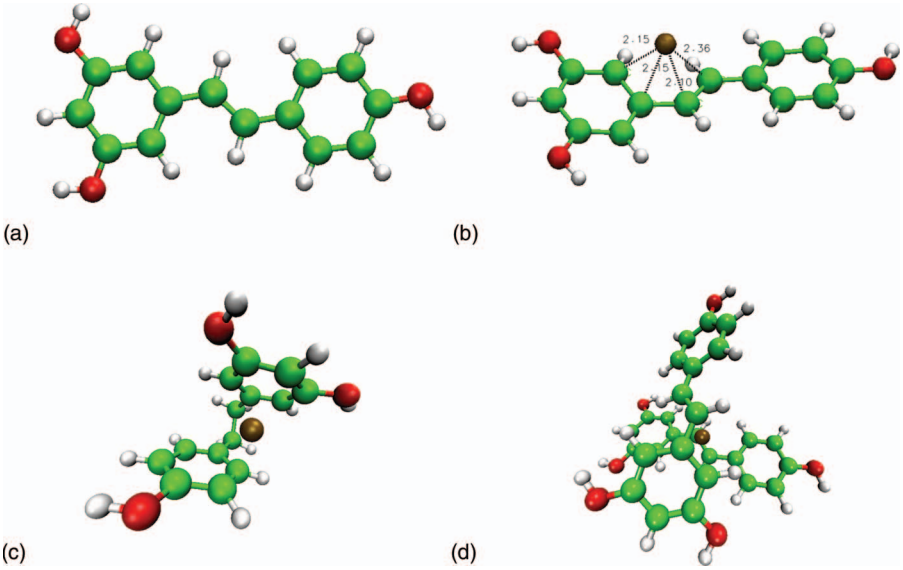

FIG. 4. Optimized structures of resveratrol (a)), resveratrol complexes (b) and d)) and $[Cu(DHResv)]^+$ (c)). Carbon is in green, hydrogen in gray, copper in orange, oxygen in red.

their instantaneous ground state (which is known to fail very far from the minimum). The forces and the stress tensor are used to determine the search directions for finding the equilibrium positions (the total energy is not taken into account). The minimum energy configuration by adopting this approach is found when the copper(I)-resveratrol complex presents a tetra-coordinated metal bound with two carbon atoms of the alkenyl moiety and two closest carbons of the adjoining resorcinol ring, as sketched in Fig. 4(b). To further check this conclusion, we performed a Bader charge analysis[33–35] of the $[Cu(Resv)]^+$ complex. This analysis uses zero flux surfaces to divide atoms, on which the charge density is a minimum perpendicular to the surface. Usually, the charge enclosed within the Bader volume is a good approximation to the total electronic charge of an atom. The calculation starts from a uniform positive charged cell, and at the end of the self-consistent procedure all four carbon atoms bound to copper gain about 0.15 eV each, while copper loses about 0.6 eV. This is a signature of the tetra-coordination between copper and the carbon atoms of resveratrol. The most stable complexes found are sketched in Fig. 4. One may note that the most stable structure for the $[Cu(Resv)]^+$ complex is slightly different from the one reported by Tamboli *et al.*,[6] though maintaining the basic binding features, possibly due to the upgraded computational approach presently adopted. In all the investigated structures, the copper atom is tightly bound to resveratrol, with binding energy decreasing from 4.931 eV in the $[Cu(Resv)]^+$ complex to 4.05 eV in the $[Cu(Resv)_2]^+$ complex. The binding energy calculations are referred to charged $(Resv)^{+\bullet}$ and neutral metal (Cu or (Resv)Cu) fragments. In other words we guessed that the positive charge remains on the departing ligand as this is the lowest dissociation limit. This is due to the fact that resveratrol first ionization energy is lower than copper ionization energy. We performed the calculations of these first ionization energies finding that resveratrol has an ionization energy of 4.28 eV, while for copper is 7.73 eV, thus confirming our working hypothesis.

DFPT, as described in Sec. III, has been applied to the calculation of the vibrational spectrum of the resveratrol complexes previously shown. Since first-principles methods necessarily involve approximations, the most important of which, in the vibrational analysis of molecules and solids, is the approximate form of the exchange-correlation interaction, it is important to validate the calculations against experimental data. To compare the theoretical spectrum with the experimental measurements, the calculated vibrational eigenvalues have been broadened with a Gaussian function with FWHM equal to 35 cm^{-1}. The theoretical spectra are normalized to the height of the experimental maximum peak in both cases. It is worthy to note that no shift of the frequency has been used, differently from what is usually done when comparing experimental data with vibrational spectra calculated by using Gaussians basis sets, which overestimate the frequencies. For the sake of comparison GTO-based DFT calculations have been performed as well. The calculated IR spectra reported in Figs. S2–S7 of the supplementary material[27] are indeed found to require scaling factors to provide matching with the positions of the experimental IRMPD bands.

The comparison between theory and experiment in Figs. 5 and 6 shows fair agreement at both low (1100–1900 cm^{-1}) and high (3500–3700 cm^{-1}) frequencies, corresponding to the so-called fingerprint and OH stretching region. However, particularly in the fingerprint region, several somewhat weak bands are predicted that are not represented in the experimental spectrum. It is possible that the intensity of these bands is predicted too high by theory. One should in fact consider that band intensities, as obtained by the described theoretical calculations, reflect the coupling with the electromagnetic field by means of Born charges. These charges represent an approximation rendering the interaction between the IR field and the vibrational normal modes, which is not exactly a model for the IRMPD process. Indeed, it is not uncommon that small absorptions may be missing in

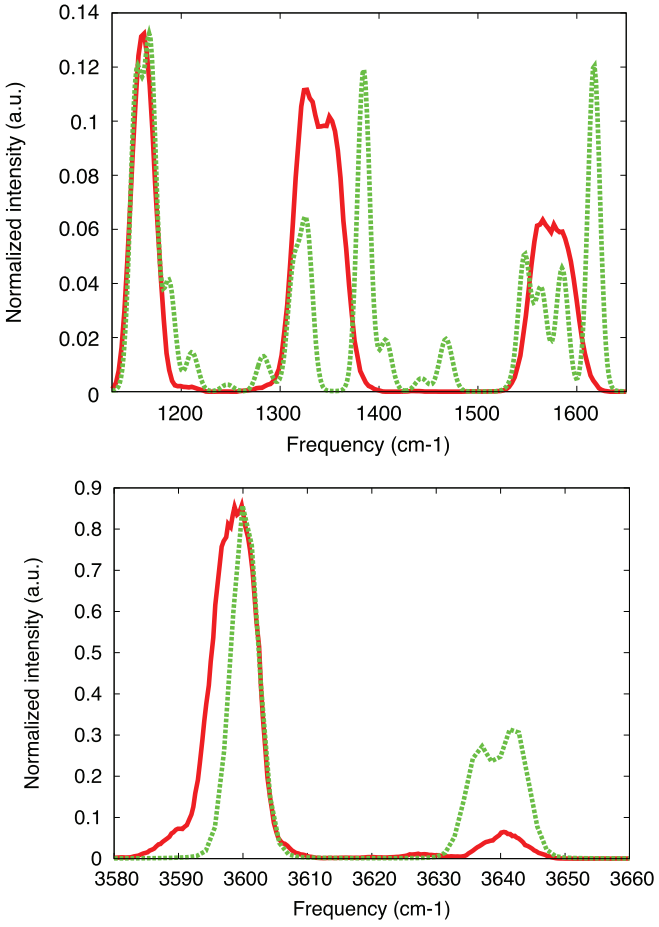

FIG. 5. Calculated (green-dashed line) infrared spectra of $(Resv)^{+\bullet}$ depicted in Fig. 4(a) for low (a) and high (b) vibrational frequencies compared to our experimental measurements (red line). Intensity values, normalized to the maximum experimental peak, are in arbitrary units.

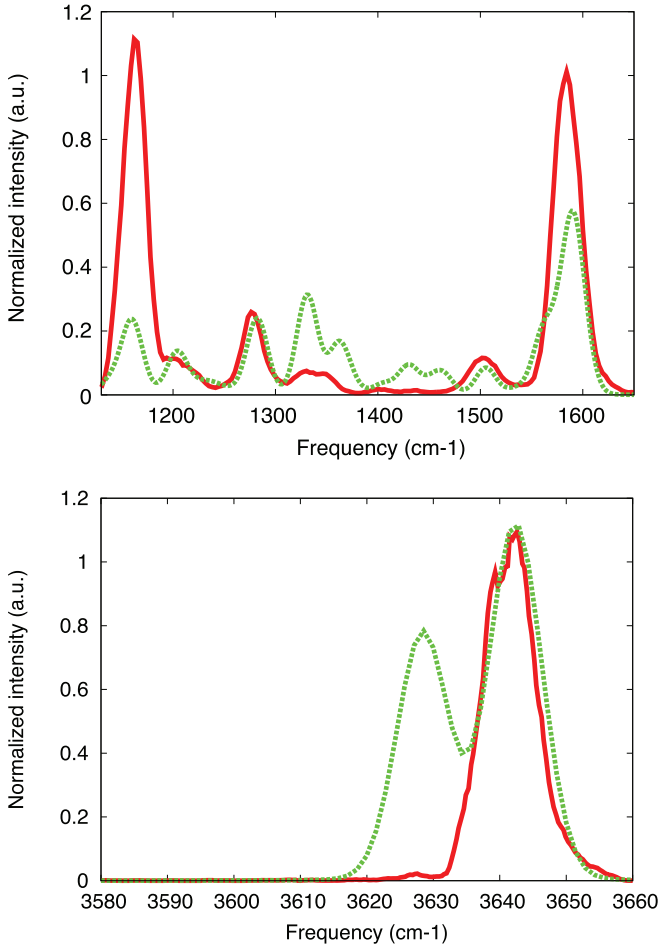

FIG. 6. Calculated (green-dashed line) infrared spectra of $[Cu(Resv)_2]^+$ depicted in Fig. 4(d) for low (a) and high (b) vibrational frequencies compared to our experimental measurements (red line). Intensity values, normalized to the maximum experimental peak, are in arbitrary units.

IRMPD spectra due to the multiphotonic nature of the process and the requirement of an efficient intramolecular vibrational relaxation.[14]

On the basis of the simulated IR spectra the major features of the experimental spectra of $(Resv)^{+\bullet}$ and$[Cu(Resv)_2]^+$ can be compared. The pronounced IRMPD feature at 1164 cm^{-1} in the spectrum of $[Cu(Resv)_2]^+$ finds a counterpart in the most active band of $(Resv)^{+\bullet}$ at 1156 cm^{-1}. At nearly the same frequency, 1167 cm^{-1}, an IRMPD band is also detected for $[Cu(Resv)]^+$. In all cases this feature encompasses in plane OH and CH bending vibrations. The wide feature in the IRMPD spectrum of $(Resv)^{+\bullet}$ at 1323–1343 cm^{-1} is associated to ring deformation and νCO modes. The corresponding bands in the IRMPD spectrum of $[Cu(Resv)_2]^+$ are noticeably less active. At higher frequency a strong, wide band of $(Resv)^{+\bullet}$ at 1573 cm^{-1} is matched by the feature at 1583 cm^{-1} in the IRMPD spectrum of $[Cu(Resv)_2]^+$. A noticeable feature for $[Cu(Resv)]^+$ at 1567 cm^{-1} is also recorded in this range. As also observed by the animation of the calculated IR modes, the active vibrations here involve local modes with major νCC character. Interestingly, two marked features at 1278 and 1503 cm^{-1} appear in the IRMPD spectrum of $[Cu(Resv)_2]^+$ that are not seen in the spectrum of $(Resv)^{+\bullet}$. The first one at 1278 cm^{-1} contains a major contribution of νCO vibrations of the two para-hydroxyphenyl units coupled with in plane CH bending. The corresponding mode in $(Resv)^{+\bullet}$ is calculated at 1310 cm^{-1}, experimentally active within the wide feature at 1323–1343 cm^{-1}. This shift to higher frequency is likely a consequence of increased double bond character of the CO bond of the *para*-hydroxyphenyl group in $(Resv)^{+\bullet}$, an effect of resonance charge and spin delocalization. From the comparison with the matching band in calculated IR spectrum the band at 1503 cm^{-1} is attached to one of several modes of ring deformation and νCC. These highly qualitative observations may be extended to the νOH features. The computed IR spectrum of $(Resv)^{+\bullet}$ allows us to assign the IRMPD band at 3601 cm^{-1} to the νOH mode of the para-hydroxyphenyl group while νOH of the dihydroxyphenyl group absorbs at 3643 cm^{-1}. The lower activity of the latter modes is also predicted by the calculations. Moving to the $[Cu(Resv)_2]^+$, once again only modest changes are observed with νOH appearing at 3643 cm^{-1} in the experimental spectrum. As also shown in Fig. 6(b), according to the computed IR spectra individual resonances for the stretching modes of the OH bonds of the two ligands spread over a 17 cm^{-1} range (the same value has been obtained in the IR spectrum reported in Fig. 5S). It

appears that in the experimental spectrum these modes coalesce into a single band whose width is consistent with a rather narrower frequency span. With regard to the $[Cu(Resv)]^+$ complex, the corresponding figure reporting the calculated IR spectra together with the experimental IRMPD spectrum is not included in this text because, as explained earlier, the complete experimental spectrum was not available due to the meager photodissociation activity of this complex. However, for the sake of completeness, this information is provided in the supplementary material (Figs. 5S and 6S).[27] Overall, the matching observed between the experimental IRMPD spectra and the calculated IR spectra for the optimized structures of $(Resv)^{+\bullet}$ and $[Cu(Resv)_2]^+$ complex supports the structural assignment provided by the computational method. Noteworthy, the OH-stretching frequencies in the region 3580–3660 cm^{-1} clearly distinguishable in Fig. 5(b) (see Fig. 3(a)) for experiments) for the pristine resveratrol molecule become almost degenerate and move to higher vibrational frequencies in the case of copper binding (see Fig. 6(b)). The very small shift toward higher frequency of the OH-stretching modes upon adsorption of copper (less than 1%), more evident in Figs. 3(b) and 3(c), can be attributed to the charge redistribution in the resveratrol molecule. Nevertheless, a Bader analysis of the charge density[35] shows that the charge on the spatially far three hydroxyl groups are left unchanged. The small frequency shift found in the OH vibrational frequencies cannot thus be due to a direct change in the OH charge density, rather to a slight stiffening of this bond due to long-range electrostatic interactions caused by the localized charge transfer.

V. CONCLUSIONS

Copper(I) complexes with resveratrol ligands have been found amenable to IRMPD spectroscopy. The experimental IRMPD spectra have yielded the IR signatures of the selected species isolated in the gas phase. In parallel, the geometric features of the sampled ions have been examined by DFT calculations and the optimized structures have been obtained. Energy gradient calculations with respect to atomic displacements and ensuing analysis have provided reference IR spectra validating the structural assignment and aiding the interpretation of the observed vibrational features. The combined experimental evidence and computational results point to copper(I) complexes engaging the π-electron frame of the resveratrol skeleton rather than the oxygen lone pairs in the coordination to the transition metal ion.

The IRMPD features of both $[Cu(Resv)]^+$ and $[Cu(Resv)_2]^+$ complexes display significant analogies with the IRMPD spectrum of ionized resveratrol which presents three pronounced bands at 1156, 1323–1343, and 1573 cm^{-1} in the mid IR region and active modes at 3601 and 3643 cm^{-1} in the OH stretching region. The dominant contribution of resveratrol modes in the inspected spectral regions is expected. At the same time the observed analogies seem to suggest a comparable perturbation of neutral resveratrol upon binding of $[Cu(Resv)]^+$ as well as upon ionization by electron loss. The present investigation may open the way to a systematic investigation of charged complexes of transition metals with bioactive molecules in an isolated state,[10,36–44] hopefully contributing to elucidate the factors governing their biological function.

ACKNOWLEDGMENTS

Financial support by the Italian MIUR (Project No. 2009W2W4YF_004), by Sapienza University (Rome) is gratefully acknowledged. B.C., M.E.C., and S.F. thank Philippe Maitre, Jean-Michel Ortega, and the European Commission for access to the CLIO facility. S.T. acknowledges that this work made use of the facilities of both HECToR, the UK's national high-performance computing service, which is provided by UoE HPCx Ltd at the University of Edinburgh, Cray Inc and NAG Ltd, and funded by the Office of Science and Technology through EPSRC's High End Computing Programme and AURORA (Bruno Kessler Foundation, Trento). Furthermore, S.T. acknowledges logistic support from the Institute of Advanced Studies of the University of Bologna.

APPENDIX: THEORETICAL AND COMPUTATIONAL METHODS

In this Appendix we provide more details on the implementation of density functional perturbation theory (DFPT),[12] used for the calculation of the resveratrol-copper complexes harmonic frequencies investigated in this work. Within DFPT, the second derivative of the total energy E can be calculated by using the Hellmann–Feynman theorem as

$$\frac{\partial^2 E}{\partial \mathbf{R}_i \partial \mathbf{R}_j} = \int \frac{\partial \rho_{\mathbf{R}}(\mathbf{r})}{\partial \mathbf{R}_j} \frac{\partial V_{\mathbf{R}}(\mathbf{r})}{\partial \mathbf{R}_i} d\mathbf{r} + \int \rho_{\mathbf{R}}(\mathbf{r}) \frac{\partial^2 V_{\mathbf{R}}(\mathbf{r})}{\partial \mathbf{R}_i \partial \mathbf{R}_j} d\mathbf{r} + \frac{\partial^2 E_{ion}(\mathbf{R})}{\partial \mathbf{R}_i \partial \mathbf{R}_j}, \quad \text{(A1)}$$

where $V_{\mathbf{R}}(\mathbf{r})$ and $E_{ion}(\mathbf{R})$ are the ion-electron and ion-ion interactions, respectively, and $\partial \rho_{\mathbf{R}}(\mathbf{r})/\partial \mathbf{R}_i$ is the derivative of the ground-state charge density with respect to the ion displacement. Within LR-DFPT, the response function $\partial \rho_{\mathbf{R}}(\mathbf{r})/\partial \mathbf{R}_i$, can be linearized by first-order perturbation of the Kohn–Sham density:[45]

$$\Delta\rho(\mathbf{r}) = 4Re \sum_{n=1}^{N/2} \psi_n^*(\mathbf{r}) \Delta\psi_n(\mathbf{r}). \quad \text{(A2)}$$

The Hamiltonian in this approximation reads:

$$(H_{KS} - \epsilon_n)|\Delta\psi_n\rangle = -(\Delta V_{KS} - \Delta\epsilon_n)|\psi_n\rangle. \quad \text{(A3)}$$

In Eq. (A3) H_{KS} is the unperturbed Kohn–Sham Hamiltonian, and ΔV_{KS} is the first-order correction to the Kohn–Sham potential

$$V_{KS}(\mathbf{r}) = V(\mathbf{r}) + \int \frac{\rho(\mathbf{r}')}{|\mathbf{r} - \mathbf{r}'|} d(\mathbf{r}') + v_{xc}, \quad \text{(A4)}$$

where v_{xc} is the exchange-correlation potential and $\Delta\epsilon_n = \langle\psi_n|\Delta V_{KS}|\psi_n\rangle$ is the first-order perturbation of the Kohn–Sham eigenvalue. Eqs. (A1), (A2), and (A3) form a set of linear equations which can be solved self-consistently as in the case of the unperturbed Kohn–Sham equations. Noteworthy, at variance with standard perturbative approaches the sum

on Eq. (A2) is only on the occupied states. This feature decreases substantially the computational cost of the calculation. Given the ground-state density and the linear response function, from Eq. (A1) one can calculate by diagonalization the vibrational eigenmodes and eigenvalues as well as the intensity of the infrared active modes (see Ref. 12 for further details). The latter can be obtained by calculating the Born effective charges $Z^*_{\alpha\beta}(i)$, measuring the coupling between the atomic displacement and the electric perturbation field, as

$$I(\omega) = \sum_{\alpha=1}^{3} \left| \sum_{i=1}^{M} \sum_{\beta=1}^{3} Z^*_{\alpha\beta}(i) e_\beta(i) \right|^2, \tag{A5}$$

where $e_\beta(i)$ is the vibrational eigenmode of atom i along the Cartesian coordinate β. In particular, the tensor $Z^*_{\alpha\beta}(i)$ accounts for the change in the system polarization and is calculated via DFPT as the second derivative of the energy with respect to the atomic displacement and the total (induced and external) electric field.[12,25,46] It contains thus important information on the electronic properties of the system and on the coupling between external fields and vibrational motion.

Finally, we would like to comment on the computational cost of performing these *ab initio* simulations. The plane wave DFT calculations of the IR spectra and of the optimization procedure to find the most stable structures according to our level of theory presented above required roughly 10^5 CPU hours on modern 2.3 GHz processors of a high-end computing terascale resource, which is a lot more expensive than the computational cost of GTO-based DFT calculations.

[1] S. Penumathsa and N. Maulik, Can. J. Physiol. Pharmacol. **87**, 275 (2009).
[2] S. J. Park, F. Ahmad, A. Philp, K. Baar, T. Williams, H. Luo, H. Ke, H. Rehmann, R. Taussig, A. L. Brown, M. K. Kim, M. A. Beaven, A. B. Burgin, V. Manganiello, and J. Chung, Cell **148**, 421 (2012).
[3] Y. Hu, J. Wang, and Q. Liu, Free Radic. Biol. Med. **51**, 250 (2011).
[4] S. Quideau, D. Deffieux, C. Douat-Casassus, and L. Pouységu, Angew. Chem. Int. Ed. **50**, 586 (2011).
[5] Y. J. Shang, Y. P. Qian, X. D. Liu, F. Dai, X. L. Shang, W. Q. Jia, Q. Liu, J. G. Fang, and B. Zhou, J. Org. Chem. **74**, 5025 (2009).
[6] V. Tamboli, A. Defant, I. Mancini, and P. Tosi, Rapid Commun. Mass Spectrom. **25**, 526 (2011).
[7] J. Oomens, B. G. Sartakov, G. Meijer, and G. von Helden, Int. J. Mass Spectrom. **254**, 1 (2006).
[8] T. D. Fridgen, Mass Spectrom. Rev. **28**, 586 (2009).
[9] J. Roithova, Chem. Soc. Rev. **41**, 547 (2011).
[10] M. A. Duncan, Int. J. Mass Spectrom. **272**, 99 (2008).
[11] L. MacAleese and P. Maitre, Mass Spectrom. Rev. **26**, 583 (2007).
[12] S. Baroni, S. de Gironcoli, A. D. Corso, and P. Giannozzi, Rev. Mod. Phys. **73**, 515 (2001).
[13] L. MacAleese, S. Aude, T. B. McMahon, J. M. Ortega, D. Scuderi, J. Lemaire, and P. Maître, Int. J. Mass Spectrom. **249/250**, 14 (2006).
[14] R. K. Sinha, P. Maître, S. Piccirillo, B. Chiavarino, M. E. Crestoni, and S. Fornarini, Phys. Chem. Chem. Phys. **12**, 9794 (2010).
[15] G. Kresse and J. Hafner, Phys. Rev. B **47**, 558 (1993).
[16] G. Kresse and J. Hafner, Phys. Rev. B **49**, 14251 (1994).
[17] G. Kresse and J. Furthmüller, Comput. Mater. Sci. **6**, 15 (1996).
[18] G. Kresse and D. Joubert, Phys. Rev. B **59**, 1758 (1999).
[19] P. E. Blochl, Phys. Rev. B **50**, 17953 (1994).
[20] J. P. Perdew, K. Burke, and M. Ernzerhof, Phys. Rev. Lett. **77**, 3865 (1996).
[21] M. J. Frisch, G. W. Trucks, and H. B. Schlegel, *et al.*, GAUSSIAN 03, Revision C.02, Gaussian, Inc., Wallingford, CT, 2004.
[22] M. W. Schmidt, K. K. Baldridge, J. A. Boatz, S. T. Elbert, M. S. Gordon, J. H. Jensen, S. Koseki, N. Matsunaga, K. A. Nguyen, S. Su, T. L. Windus, M. Dupuis, and J. A. Montgomery, J. Comput. Chem. **13**, 1347 (1993).
[23] S. Tosoni, C. Tuma, J. Sauer, B. Civalleri, and P. Ugliengo, J. Chem. Phys. **127**, 154102 (2007).
[24] J. Perdew, J. Chevary, S. Vosko, K. Jackson, M. Pederson, D. Singh, and C. Fiolhais, Phys. Rev. B **46**, 6671 (1992).
[25] J. H. D. Karhánek and T. Buûko, J. Phys.: Condens. Matter **22**, 265006 (2010).
[26] J. Paier, M. Marsman, and G. Kresse, J. Chem. Phys. **127**, 024103 (2007).
[27] See supplementary material at http://dx.doi.org/10.1063/1.4732583 for a comparison between plane waves DFPT and GTO-based DFT spectra.
[28] P. Milko, J. Roithova, D. Schröder, J. Lemaire, H. Schwarz, and M. C. Holthausen, Chem. Eur. J. **14**, 4318 (2008).
[29] J. Perdew and A. Zunger, Phys. Rev. B **23**, 5048 (1981).
[30] F. Tran, R. Laskowski, P. Blaha, and K. Schwartz, Phys. Rev. B **75**, 115131 (2007).
[31] D. M. Goldberg, J. Yan, E. Ng, E. P. Diamandis, A. Karumanchiri, G. Soleas, and A. L. Waterhouse, Anal. Chem. **66**, 3959 (1994).
[32] F. Billes, I. Mohammed-Ziegler, H. Mikosch, and E. Tyihak, Spectrochim. Acta A: Mol. Biomol. Spectrosc. **68**, 669 (2007).
[33] G. Henkelman, A. Arnaldsson, and H. Jonsson, Comput. Mater. Sci. **36**, 254 (2006).
[34] E. Sanville, S. D. Kenny, R. Smith, and G. Henkelman, J. Comp. Chem. **28**, 899 (2007).
[35] W. Tang, E. Sanville, and G. Henkelman, J. Phys.: Condens. Matter **21**, 084204 (2009).
[36] M. W. Forbes, M. F. Bush, N. C. Polfer, J. Oomens, R. C. Dunbar, E. R. Williams, and R. A. Jockusch, J. Phys. Chem. A **111**, 11759 (2007).
[37] N. C. Polfer, J. Oomens, D. T. Moore, G. von Helden, G. Meijer, and R. C. Dunbar, J. Am. Chem. Soc. **128**, 517 (2006).
[38] U. H. Verkerk, J. Zhao, I. S. Saminathan, J. K.-C. Lau, J. Oomens, A. C. Hopkinson, and K. W. M. Siu, Inorg. Chem. **51**, 4707 (2012).
[39] R. C. Dunbar, J. D. Steill, and J. Oomens, Phys. Chem. Chem. Phys. **12**, 13383 (2010).
[40] R. C. Dunbar, J. D. Steill, N. C. Polfer, and J. Oomens, J. Phys. Chem. A **113**, 845 (2009).
[41] N. C. Polfer, J. Oomens, and R. C. Dunbar, Phys. Chem. Chem. Phys. **8**, 2744 (2006).
[42] A. Lagutschenkov, R. K. Sinha, P. Maitre, and O. Dopfer, J. Phys. Chem. A **114**, 11053 (2010).
[43] A. Lagutschenkov, U. J. Lorenz, and O. Dopfer, Int. J. Mass Spectrom. **308**, 316 (2011).
[44] S. Chakraborty and O. Dopfer, Chem. Phys. Chem. **12**, 1999 (2011).
[45] A. Messiah, *Quantum Mechanics* (Courier Dover, 1999).
[46] P. Giannozzi and S. Baroni, J. Chem. Phys. **100**, 8537 (1994).